Check for updates

Earth's Future

RESEARCH ARTICLE
10.1029/2022EF002708

Constraining CMIP6 Projections of an Ice-Free Arctic Using a Weighting Scheme

Jiazhen Zhao[1], Shengping He[2,3,4], Huijun Wang[1,3,5], and Fei Li[2]

[1]Key Laboratory of Meteorological Disaster, Ministry of Education/Joint International Research Laboratory of Climate and Environment Change (ILCEC)/Collaborative Innovation Center on Forecast and Evaluation of Meteorological Disasters (CIC-FEMD), Nanjing University of Information Science & Technology, Nanjing, People's Republic of China, [2]Geophysical Institute, University of Bergen and Bjerknes Centre for Climate Research, Bergen, Norway, [3]Nansen-Zhu International Research Centre, Institute of Atmospheric Physics, Chinese Academy of Sciences, Beijing, People's Republic of China, [4]Nansen Environmental and Remote Sensing Center and Bjerknes Centre for Climate Research, Bergen, Norway, [5]Southern Marine Science and Engineering Guangdong Laboratory (Zhuhai), Zhuhai, People's Republic of China

Abstract Employing a model democracy in which each model is equally weighted may lead to a poor estimation of the true uncertainty in climate projections from phase 6 of the Coupled Model Intercomparison Project (CMIP6). The improvement and increase in number of CMIP6 models compared with previous phases of CMIP indicate that both model skill and independence need to be considered to provide convincing projections. In this study, we use a weighting scheme, which weights both the skill and independence of multi-model simulations, to efficiently constrain the large uncertainty in the projection of the timing of an ice-free Arctic. The uncertainty-constrained projections of CMIP6 show that the multi-model spread of the projected first year of an ice-free Arctic can be reduced by about 29 years under the Shared Socioeconomic Pathway (SSP)3–7.0 scenario (a regional rivalry scenario), indicating a faster tendency to an ice-free Arctic summer than projections based solely on model democracy. A fossil-fuel-based development scenario (i.e., SSP5-8.5) leads to an ice-free Arctic before the 2070s (ranging from 2038 to 2071), while an ice-free Arctic occurs slightly later (by ~10 years) under the SSP2-4.5 scenario (i.e., intermediate scenario) and the SSP3-7.0 scenario, but is inevitable this century. The sustainable development scenario (i.e., SSP1-2.6) is likely to prevent the occurrence of an ice-free Arctic. Internal variability strongly affects the projection estimated by the equally weighted ensemble; however, it has a negligible impact on the results obtained by the weighting scheme, thereby indicating that the results of this study are robust and convincing.

Plain Language Summary Climate models are a key tool used by scientists to estimate climate changes in the future. However, the outputs of such models carry inherent uncertainties that can affect the confidence in projections. These uncertainties may not be appropriately estimated by simple and traditional methods that do not adequately consider the model skill or independence (i.e., similarity to other models). In this study, we found that the uncertainties in Arctic sea-ice projections can be largely reduced if the outputs of climate models are weighted according to their performance and independence. By doing so, we can increase the level of confidence in estimating the year when the Arctic is likely to see its first ice-free summer (sea-ice extent below 1×10^6 km^2). It is indicated that a sustainable development scenario may avoid an ice-free Arctic. In contrast, a fossil-fuel-based development scenario will lead to an ice-free Arctic before the 2070s (ranging from 2038 to 2071); and an ice-free Arctic will occur slightly later (by ~10 years) under an intermediate or regional rivalry scenario, but is still inevitable this century.

Key Points:

- The performance and interdependence of climate models may lead to a poor estimation of the true uncertainty in climate projections
- A weighting scheme considering both model skill and independence can reduce the spread in the first year of an ice-free Arctic by ~29 years
- The weighted spread indicates that the first year of an ice-free Arctic is likely to occur during 2040–2072 under the SSP3-7.0 scenario

Supporting Information:

Supporting Information may be found in the online version of this article.

Correspondence to:

S. He,
Shengping.He@uib.no

Citation:

Zhao, J., He, S., Wang, H., & Li, F. (2022). Constraining CMIP6 projections of an ice-free Arctic using a weighting scheme. *Earth's Future*, *10*, e2022EF002708. https://doi.org/10.1029/2022EF002708

Received 15 FEB 2022
Accepted 28 SEP 2022
Corrected 4 NOV 2022

This article was corrected on 4 NOV 2022. See the end of the full text for details.

Author Contributions:

Conceptualization: Shengping He, Huijun Wang
Formal analysis: Jiazhen Zhao, Shengping He
Methodology: Jiazhen Zhao, Shengping He
Software: Jiazhen Zhao, Shengping He

© 2022 The Authors. Earth's Future published by Wiley Periodicals LLC on behalf of American Geophysical Union. This is an open access article under the terms of the Creative Commons Attribution-NonCommercial-NoDerivs License, which permits use and distribution in any medium, provided the original work is properly cited, the use is non-commercial and no modifications or adaptations are made.

1. Introduction

The rapid warming in the Arctic at a rate more than double that of the global average has contributed to remarkable decreases in Arctic sea ice during recent decades (Cohen et al., 2014; Notz & SIMIP Community, 2020). According to the National Snow and Ice Data Center (NSIDC) Sea Ice Index version 3 (Fetterer et al., 2017), the September mean Arctic sea-ice extent (SIE; defined as the area covered by sea ice with a concentration of at least 15%) reached a record low of 3.57 million km^2 in 2012, and the second-lowest value at 4.00 million km^2 in 2020. State-of-the-art climate models have projected that the Arctic sea ice is very likely to continue to decline over the coming decades (IPCC, 2021; Notz & SIMIP Community, 2020; Song, 2016). Therefore, the timing of when an ice-free Arctic summer will eventually occur, which will have substantial impacts on the Arctic environment,

23284277, 2022, 10, Downloaded from https://agupubs.onlinelibrary.wiley.com/doi/10.1029/2022EF002708 by Universitetsbiblioteket I, Wiley Online Library on [29/12/2022]. See the Terms and Conditions (https://onlinelibrary.wiley.com/terms-and-conditions) on Wiley Online Library for rules of use; OA articles are governed by the applicable Creative Commons License

23284277, 2022, 10, Downloaded from https://agupubs.onlinelibrary.wiley.com/doi/10.1029/2022EF002708 by Universitetsbiblioteket1, Wiley Online Library on [29/12/2022]. See the Terms and Conditions (https://onlinelibrary.wiley.com/terms-and-conditions) on Wiley Online Library for rules of use; OA articles are governed by the applicable Creative Commons License

Writing – original draft: Jiazhen Zhao, Shengping He, Huijun Wang
Writing – review & editing: Jiazhen Zhao, Shengping He, Huijun Wang, Fei Li

marine ecosystems and even the global climate (Cohen et al., 2020; Francis & Vavrus, 2012; Wang et al., 2021), has become a prominent societal and scientific concern.

It is widely agreed that an ice-free Arctic summer, defined as when the Arctic SIE drops below 1×10^6 km^2 (Jahn, 2018; Liu et al., 2013; Wang & Overland, 2009, 2012), is likely to occur before the end of the 21st century (Boé et al., 2009; Jahn, 2018; Sigmond et al., 2018). Many recent studies have indicated that the Arctic will likely become ice free in summer around the middle of this century (Laliberté et al., 2016; Liu et al., 2013; Notz & SIMIP Community, 2020) or even earlier—in the 2030s, for instance (Bonan, Schneider, et al., 2021; DeRepentigny et al., 2020; Diebold & Rudebusch, 2021; Wang et al., 2021; Wang & Overland, 2009). The latest Intergovernmental Panel for Climate Change (IPCC) Assessment Report (AR6) has stated, based on an equally weighted multi-model mean, that "*The Arctic is likely to be practically sea ice free in September at least once before 2050 under the five illustrative scenarios considered in this report, with more frequent occurrences for higher warming levels.*"

However, the projected timing of an ice-free Arctic still carries large uncertainties (Jahn, 2018; Jahn et al., 2016; Laliberté et al., 2016; Liu et al., 2013; Wang et al., 2021). The uncertainty arises primarily from internal variability and the different structures of current global climate models (GCMs) (Årthun et al., 2021; Bonan, Lehner, & Holland, 2021; DeRepentigny et al., 2020; Notz & SIMIP Community, 2020). In terms of the projected timing of an ice-free Arctic summer, internal variability alone can lead to uncertainty of about two decades (Jahn et al., 2016). Additionally, scenario uncertainty can add at least five more years (Jahn et al., 2016). Taken together, this already clearly indicates that such an uncertainty may strongly affect the level of confidence in projections. To reduce this uncertainty, scientists have tried using a sub-selection of well-performing models (Docquier & Koenigk, 2021; Laliberté et al., 2016; Liu et al., 2013; Notz & SIMIP Community, 2020; Thackeray & Hall, 2019). For instance, by omitting models with poor skill in simulating a variety of sea-ice related diagnostics (e.g., seasonal sea-ice albedo feedback, sea-ice thickness), Thackeray and Hall (2019) showed that the spread in the timing of an ice-free Arctic in September could be narrowed to a 20-year window spanning from the 2040s to the 2060s. The above studies imply that the estimated timing of an ice-free Arctic summer may depend on the method used, indicating the need to utilize advanced approaches to provide more convincing projections.

Emergent constraints, which rely on the linear relationship between the observable aspects of the current climate system and the future climate change across GCMs, have been previously used to constrain the uncertainty of Arctic sea-ice projections (Bonan, Schneider, et al., 2021; Liu et al., 2013; Wang et al., 2021). For example, using a statistical framework that relates future sea-ice area (SIA; quantified as the grid-cell area multiplied by the sea-ice concentration) to present-day SIA and to the local sea-ice sensitivity, together with the application of emergent constraints, Bonan, Schneider, et al. (2021) indicated that the first year of an ice-free Arctic under a high-emissions scenario is likely to occur between 2036 and 2056, which is an advancement of about 10–35 years relative to the projection without uncertainty constraint. In addition, a recent study using emergent constraints pointed out that the chance of an ice-free Arctic summer to occur with approximately 1.9°C warming above the pre-industrial level can reach up to 80% (Wang et al., 2021).

It is noteworthy that the approach used in studies that have constrained the projection uncertainty by selecting well-performing models involved each selected model being equally weighted, regardless of the level of interdependence with other models, which may have led to overfitting in the projections generated. Additionally, in studies that have constrained the projection uncertainty through the application of emergent constraints to all available simulations, there may have been overconfidence in the projection results if all the simulations had structurally similar problems (Knutti et al., 2017). Considering the above limitations, Knutti et al. (2017) proposed an alternative approach in which both the skill and independence of climate models are weighted to reduce the uncertainty in projected Arctic sea-ice variability. Through applying such a weighting scheme to all available simulations from the third and fifth phases of the Coupled Model Intercomparison Project (CMIP3/CMIP5), many previous studies have proven that this method is able to efficiently constrain model biases and narrow the spread of projection by different climate models (Knutti et al., 2017; Lorenz et al., 2018; Merrifield et al., 2019; Tong et al., 2020). One of the main advantages of the weighting scheme is that it takes into account the interdependence of models. It is well known that the current state-of-the-art climate models are largely interdependent (Knutti et al., 2013; Masson & Knutti, 2013; Sanderson et al., 2015b, 2017). Models developed by the same community with different resolutions (e.g., MPI-ESM-HR and MPI-ESM-LR), for instance, have many similarities. Also, it was suggested by Knutti et al. (2017) that model interdependence will become more prevalent in future phases of

23284277, 2022, 10, Downloaded from https://agupubs.onlinelibrary.wiley.com/doi/10.1029/2022EF002708 by Universitetsbiblioteket I, Wiley Online Library on [29/12/2022]. See the Terms and Conditions (https://onlinelibrary.wiley.com/terms-and-conditions) on Wiley Online Library for rules of use; OA articles are governed by the applicable Creative Commons License

CMIP since the total number of models from all communities as well as individual models from the same institute will both increase. Taking CMIP6, for example, the National Center for Atmospheric Research has provided four versions of the Community Earth System Model (CESM)—namely, CESM2, CESM2-FV2, CESM2-WACCM, and CESM2-WACCM-FV2. In addition, climate models share a large amount of code. For example, there is a lot of common code between TaiESM1 and CESM1.2.2 owing to the limited manpower and expertise in climate research in Taiwan (Lee et al., 2020). This interdependence of models can potentially lead to poor estimation of the uncertainty in climate projections (Brunner et al., 2020; Herger et al., 2018; Zhao et al., 2022), which has been commonly overlooked by previous studies, including the IPCC assessment reports. Knutti et al. (2017), one of the pioneering groups to apply a weighting scheme to Arctic sea-ice projections, argued that (a) weighted projections indicate a more rapid sea-ice decline than unweighted projections, and (b) the weighting scheme is more crucial for reducing the uncertainty in climate projections than a model democracy in which each model is equally weighted.

The present study was inspired by this pioneering work of Knutti et al. (2017) carried out on the basis of the CMIP3 and CMIP5 archives. More specifically, there were three major motivations behind us conducting this follow-up research. First, Knutti et al. (2017) did not estimate the timing of an ice-free Arctic. Rather, they investigated the variation in September SIE under a medium-emissions scenario (Representative Concentration Pathway [RCP]) 4.5) and stated that "*The weighted projection points to near ice-free September conditions by 2100 for RCP4.5.*" However, recent studies have indicated that ice-free conditions in September are likely to occur much earlier than expected under scenarios representing equal or higher emission levels (Bonan, Schneider, et al., 2021; Wang et al., 2021). Second, the unweighted mean of the CMIP3/CMIP5 outputs underestimate the observed rates of decline in September Arctic sea ice (see black curve in Figure 1c of Knutti et al. (2017)). This may potentially lead to an overestimation of the remaining SIE in future, and hence lead to a conservative estimate of the timing of an ice-free Arctic. Third, the weighted mean of the CMIP3/CMIP5 outputs still notably underestimates the observed rates of September Arctic sea-ice loss (see red curve in their Figure 1c), showing a limited constraint of present-day simulation biases by the weighting scheme. This is likely to result from the poor skill of the CMIP3/CMIP5 models in reproducing the observed Arctic sea-ice variability, which implies a need to apply the weighting scheme to the latest state-of-the-art climate models.

The CMIP6 archive represents nearly a decade of development relative to its predecessors. It has been shown that the ensemble mean of CMIP6 simulations can successfully capture the observed rate of decline in September Arctic SIA, as well as its response to external forcing (Notz & SIMIP Community, 2020). Considering the notable improvement but increased interdependence of CMIP6 models, in this paper we report findings from applying a weighting scheme to the latest CMIP6 archives to constrain the uncertainty in the projected timing of an ice-free Arctic in September during the 21st century. The hope is that the results of this study will help to address societal and scientific concerns associated with when the summertime Arctic will become ice free for the first time.

2. Data and Methods

2.1. CMIP6 Archive

Our analysis is based on all currently available CMIP6 models (Eyring et al., 2016; O'Neill et al., 2016) that have published monthly sea ice concentration (SIC), surface air temperature (SAT), sea surface temperature (SST) and sea level pressure (SLP) in both historical simulations during 1850–2014 and future projections under the Shared Socioeconomic Pathways (SSPs) of SSP1-2.6, SSP2-4.5, SSP3-7.0 and SSP5-8.5 during 2015–2100. In total, 29 different models are used in this study (Table 1) and only one ensemble member of each model is used. It is noteworthy that including more members of each model will not change the conclusions of this study, since internal variability has a negligible impact on the effect of our weighting scheme (see discussion in Section 4.2). To improve the comparability between the model outputs and the observations, all model outputs were interpolated to a regular grid resolution of 1° longitude by 1° latitude. We used the monthly SIC to calculate the monthly Arctic SIE or SIA. To illustrate climate change more clearly, three specific 30-year periods are examined: 1981–2010 (historical), 2021–2050 (near-term) and 2070–2099 (long-term).

23284277, 2022, 10, Downloaded from https://agupubs.onlinelibrary.wiley.com/doi/10.1029/2022EF002708 by Universitetsbiblioteket I, Wiley Online Library on [29/12/2022]. See the Terms and Conditions (https://onlinelibrary.wiley.com/terms-and-conditions) on Wiley Online Library for rules of use; OA articles are governed by the applicable Creative Commons License

Table 1
Details of the 29 CMIP6 Models Used in This Study

Model no.	Model name	Institution/Country
1	ACCESS-CM2	CSIRO-ARCCSS/Australia
2	ACCESS-ESM1-5	CSIRO/Australia
3	BCC-CSM2-MR	BCC-CMA/China
4	CAMS-CSM1-0	CAMS-CMA/China
5	CanESM5	CCCMA/Canada
6	CanESM5-CanOE	CCCMA/Canada
7	CAS-ESM2-0	CAS/China
8	CESM2	NCAR/USA
9	CESM2-WACCM	NCAR/USA
10	CNRM-CM6-1	CNRM-CERFACS/France
11	CNRM-CM6-1-HR	CNRM-CERFACS/France
12	CNRM-ESM2-1	CNRM-CERFACS/France
13	EC-Earth3	EC-Earth-Consortium/EU
14	EC-Earth3-Veg	EC-Earth-Consortium/EU
15	EC-Earth3-Veg-LR	EC-Earth-Consortium/EU
16	FGOALS-f3-L	LASG-IAP/China
17	FGOALS-g3	LASG-IAP/China
18	INM-CM4-8	INM/Russia
19	INM-CM5-0	INM/Russia
20	IPSL-CM6A-LR	IPSL/France
21	MIROC6	MIROC/Japan
22	MIROC-ES2L	MIROC/Japan
23	MPI-ESM1-2-HR	MPI-M/Germany
24	MPI-ESM1-2-LR	MPI-M/Germany
25	MRI-ESM2-0	MRI/Japan
26	NorESM2-LM	NCC/Norway
27	NorESM2-MM	NCC/Norway
28	TaiESM1	AS-RCEC/Taiwan
29	UKESM1-0-LL	MOHC/UK

2.2. CESM2 Large Ensemble

The CESM2 Large Ensemble (CESM2-LE; Rodgers et al., 2021) is used to assess the effect of internal variability on the results derived from the weighting scheme. The CESM2-LE consists of 100 ensemble members covering the period 1850–2100, composed of the CMIP6 historical simulations and the projections under the SSP3-7.0 scenario. The first and the second 50 of the 100 ensemble members use different forcing fields. The first 50 members follow the original CMIP6 biomass-burning protocol, which is described in the CESM2 overview paper (Danabasoglu et al., 2020). In the second 50 members, the original CMIP6 biomass-burning emissions are smoothed in time with an 11-year running mean filter. This smoothing has been shown to strongly affect the multidecadal trends in Arctic sea ice in the CESM2, through reductions in the interannual variability of the prescribed CMIP6 biomass-burning emissions (DeRepentigny et al., 2022). Only the first 50 of the 100 members are used in this study to ensure the comparability between the projections derived from the CESM2-LE and the projections obtained from the CMIP6 models under the SSP3-7.0 scenario. These members only differ from each other in their initial oceanic and atmospheric conditions (i.e., phase of the Atlantic meridional overturning circulation, atmospheric potential temperature), which ensures that each member has a unique time sequence of internal variability. The monthly SIC and SLP during 1980–2100 from CESM2-LE are used. The monthly SIC was used to calculate the monthly Arctic SIE. All ensemble outputs were interpolated to a regular $1° \times 1°$ grid.

2.3. Observations

Monthly SIC data with a regular grid resolution of $1° \times 1°$ were obtained from the Met Office's Hadley Centre Sea Ice and Sea Surface Temperature data set (HadISST 1.1; Rayner et al., 2003). Monthly SLP, SAT and SST data were obtained from the European Centre for Medium-Range Weather Forecasts (ECMWFs) fifth-generation global atmospheric reanalysis (ERA5) with a spatial resolution of $0.25° \times 0.25°$, which are currently available from January 1950 to the present day (Hersbach et al., 2020). All reanalysis data used in this study were interpolated to a regular grid resolution of $1° \times 1°$ to facilitate the comparison with the model results. Observed monthly time series of Arctic SIE and SIA were obtained from the NSIDC Sea Ice Index version 3 (Fetterer et al., 2017).

2.4. Definitions of Arctic SIE, SIA and Ice-Free Conditions

To ensure our results are comparable with previous studies, we define the timing of an ice-free Arctic as the first year when the September Arctic SIE drops below 1×10^6 km^2 (IPCC, 2013; Jahn, 2018; Laliberté et al., 2016; Sigmond et al., 2018). The SIE time series was estimated as the total area of all grid cells in the Northern Hemisphere with an SIC of at least 15%. Considering that several recent studies have also used SIA to project the timing of an ice-free Arctic summer (IPCC, 2021; Notz & SIMIP Community, 2020; Wang et al., 2021), we also present the results relevant to the Arctic SIA in Figures S1–S7 in Supporting Information S1. To calculate the time series of the SIA, we multiplied every grid-cell area by its SIC (ranging from 0.0 to 1.0) and summed up all the grid values over the Northern Hemisphere.

2.5. Multi-Model Weighting Scheme

The weighting scheme employed in this study was developed by Knutti et al. (2017) based on the work of Sanderson et al. (2015a, 2015b). It has been recommended in recent studies as an alternative to the method

23284277, 2022, 10, Downloaded from https://agupubs.onlinelibrary.wiley.com/doi/10.1029/2022EF002708 by Universitetsbiblioteket1, Wiley Online Library on [29/12/2022]. See the Terms and Conditions (https://onlinelibrary.wiley.com/terms-and-conditions) on Wiley Online Library for rules of use; OA articles are governed by the applicable Creative Commons License

of model sub-selection or emergent constraints (Brunner et al., 2020; Knutti et al., 2017; Lorenz et al., 2018; Merrifield et al., 2019; Sanderson et al., 2017; Tong et al., 2020). The weighting scheme abandons the prevailing model democracy in dealing with ensemble simulations (Knutti, 2010). Instead, it weights the multi-model simulations according to their performance and their similarities in simulating a set of diagnostics that are relevant to the projected targets. In terms of the SIE projections in this study, the weight of each GCM in the CMIP6 archive was derived based on their present-day simulations. This is plausible since the large spread in the projected sea-ice decline over the 21st century by individual GCMs mainly originates from biases in their present-day simulations (Bonan, Schneider, et al., 2021). Weighting based on present-day simulations could maximize the constraint effect on present-day biases and projection uncertainty. Models agreeing well with observations or having rare duplicates in the CMIP6 archive will be up-weighted by the weighting scheme, and vice versa. The weighted/unweighted ensemble spread, which measures the difference between the ensemble members, was calculated as a weighted/unweighted standard deviation. The mean of the weighted/unweighted ensemble can provide a relatively representative estimate of the future outcome's temporal evolution for policymakers to refer to. For a model i, its weight w_i is calculated as follows:

$$w_i = \frac{e^{-\frac{D_i^2}{\sigma_D^2}}}{1 + \sum_{j \neq i}^{M} e^{-\frac{S_{ij}^2}{\sigma_s^2}}} \tag{1}$$

where D_i is the distance of model i to the observations, S_{ij} is the distance of model i to model j, M is the total number of models, and σ_D and σ_s are the shape parameters. The root-mean-square error (RMSE) is used to represent the distance metric of D_i and S_{ij} (Knutti et al., 2017; Lorenz et al., 2018; Merrifield et al., 2019; Sanderson et al., 2017). D_i is used to estimate model i's skill weight $\left(e^{-\frac{D_i^2}{\sigma_D^2}}\right)$, with a larger value leading to a smaller skill weight, and vice versa. The S_{ij} $(j \neq i)$ is used to estimate model i's independence weight $\left(\frac{1}{1+\sum_{j \neq i}^{M} e^{-\frac{S_{ij}^2}{\sigma_s^2}}}\right)$, with a larger value leading to a larger independence weight, and vice versa. Sanderson et al. (2017) weighted the model independence according to both model-to-model distance S_{ij} and some prior knowledge about known interdependence in multi-model simulations. Different from Sanderson et al. (2017), in this study, we determined the model independence metric solely according to S_{ij} because weighting based on prior knowledge may be somewhat subjective and may lead to loss of some potentially useful information. Equation 1 indicates that model i's weight is computed as the product of its skill weight and its independence weight. To better compare the results derived from the weighting scheme with those obtained from the model democracy (i.e., each model having an equal weight of $1/M$), we normalized all model weights (i.e., the sum of unequal weights is also equal to one).

For this paper, we selected a variety of diagnostics to calculate D_i and S_{ij}, including both the temporal variability of a variable and the spatial pattern of several basic climate features (e.g., climatology, trend, interannual variability; more details on the motivation for diagnostic selection can be found in Section 2.6), such that both the temporal and the spatial distances could be calculated. The distances corresponding to different diagnostics were averaged to determine the values of D_i and S_{ij}. Since different diagnostics may create different distance magnitudes, each diagnostic distance, including both the model-to-model distances and the model-to-observation distances, was normalized by the median before it was averaged. D_i and S_{ij} were calculated with reference to the baseline period of 1980–2014, which makes observations and historical simulations more comparable.

The two shape parameters [σ_D and σ_s in Equation 1] determine how strongly the model's performance (numerator in Equation 1) and the model's similarity [denominator in Equation 1] are weighted, respectively. As suggested by Knutti et al. (2017), a large σ_D effectively converges to a model democracy that weights models equally, whereas a small σ_D tends to assign most weights to only a few models so that most models receive a near-zero weight. It is inappropriate to choose either a too small or a too large value of σ_D (see discussion in Section 2.7). σ_s represents the distance scale at which two models are considered to be similar. More details of the method can be found in Knutti et al. (2017). To estimate the two shape parameters, we utilized the same approach as Knutti et al. (2017)

23284277, 2022, 10, Downloaded from https://agupubs.onlinelibrary.wiley.com/doi/10.1029/2022EF002708 by Universitetsbiblioteket I, Wiley Online Library on [29/12/2022]. See the Terms and Conditions (https://onlinelibrary.wiley.com/terms-and-conditions) on Wiley Online Library for rules of use; OA articles are governed by the applicable Creative Commons License

through a perfect model setup, which is explained in detail in Section 2.7. The large interdependence that exists in the CMIP6 archive could make the perfect model setup work better (Lorenz et al., 2018). To test the robustness of the results derived from the weighting scheme of this study, different diagnostic sets were used to weight the models (see discussion in Section 4.1), and in each case, σ_D and σ_s were chosen separately.

2.6. Motivation for Diagnostic Choices

We used Equation 1 to obtain weighted projections of September Arctic SIE and accordingly derive the first year of an ice-free Arctic. The diagnostic variables, which were taken into account in the calculation of the model-to-observation distance and the model-to-model distance (D_i and S_{ij}, respectively), needed to be determined based on physical mechanisms (Knutti et al., 2017). In this study, instead of only focusing on the projected target (i.e., September Arctic SIE), we comprehensively considered multiple variables relevant to the projected target in the calculation of D_i and S_{ij}. Such an approach is consistent with that of Knutti et al. (2017), the motivation for which is the fact that weighting solely based on the projected target may cause overconfidence in the results (Lorenz et al., 2018). For example, if one model has poor skill in simulating the overall September Arctic sea-ice related climate but it coincidently matches well with the observed September Arctic SIE, this model would be unreasonably up-weighted if weighting is solely based on the one target variable (i.e., September Arctic SIE). On the other hand, selecting more variables should also be done cautiously because the inclusion of certain irrelevant diagnostics will tend to cause models to be weighted randomly (Knutti et al., 2017; Sanderson et al., 2017) and will eventually drive the weighting scheme toward model democracy, unless the number of models is small (Weigel et al., 2010).

In this paper, we evaluate both the model skill and independence based on several climate diagnostics (e.g., some key variables, climatology, and trend) related to the projected target (Knutti et al., 2017; Lorenz et al., 2018; Merrifield et al., 2019). To apply the weighting scheme to the projections of September Arctic SIE, Knutti et al. (2017) used the climatological mean and the trend of hemispheric September Arctic SIE, the gridded climatological mean, and the interannual variability of SAT of each month as the relevant climate. However, SIC in the Arctic, which is directly tied to the SIE (see Section 2.4), was barely taken into account by Knutti et al. (2017). Therefore, focusing on the same projected target (September SIE) as Knutti et al. (2017), we considered both SIE and SIC to estimate the weights for each model member. Although SAT and SST are closely related to sea-ice variability (Alekseev et al., 2021; Screen & Deser, 2019; Senftleben et al., 2020; Wang et al., 2021), the two variables are not used in the weighting scheme because of their intense co-variation and their close relation to SIC, which may lead to overfitting in the weighting. Given that the dynamics are also crucial to sea-ice variability (Lukovich et al., 2021; Park et al., 2018; Ricker et al., 2021), we considered an additional climate variable, the summer (June–July–August, JJA) mean SLP, which can drive the variability of September Arctic sea ice (Ding et al., 2017, 2019). Our motivation in choosing these diagnostics was based on the above physical links as well as the fact that climatology, trend and interannual variability have been commonly regarded as basic climate features in GCM assessments (Guo et al., 2021; Knutti et al., 2017; Shiru & Chung, 2021; Yang et al., 2021). Accordingly, we chose the following seven diagnostics to represent the climate that is crucial to the projections of September Arctic SIE: (a) the temporal variability of September SIE; the spatial patterns of the (b) climatology, (c) trend, and (d) interannual variability of Arctic (60°–90°N) September SIC; and the spatial patterns of the (e) climatology, (f) trend, and (h) interannual variability of Arctic JJA SLP. These diagnostics were treated as identically important in the weight estimation (see Section 2.5).

2.7. Perfect Model Setup

The two shape parameters (σ_D and σ_s) were determined based on a perfect model setup (Knutti et al., 2017). This setup enabled us to test whether the choice of the distance metrics and the diagnostics led to an overconfident weighting (Brunner et al., 2020; Knutti et al., 2017; Tong et al., 2020). Within the setup, we selected every model in turn from CMIP6 to represent the "truth", and then weighted the remaining models to predict this "truth". After the setup had been completed M times (M being the total number of models, with each model having been selected to represent the "truth" only once), we calculated the fraction of cases in which the "truth" fell between the 10th and the 90th percentiles of the "truth" prediction. Corresponding to each σ_D and σ_s, we ensured that the fraction reached at least 80%—a threshold commonly chosen to avoid overconfidence in the weighting (Brunner et al., 2020; Lorenz et al., 2018; Merrifield et al., 2019; Sanderson et al., 2017). We selected eight targets for

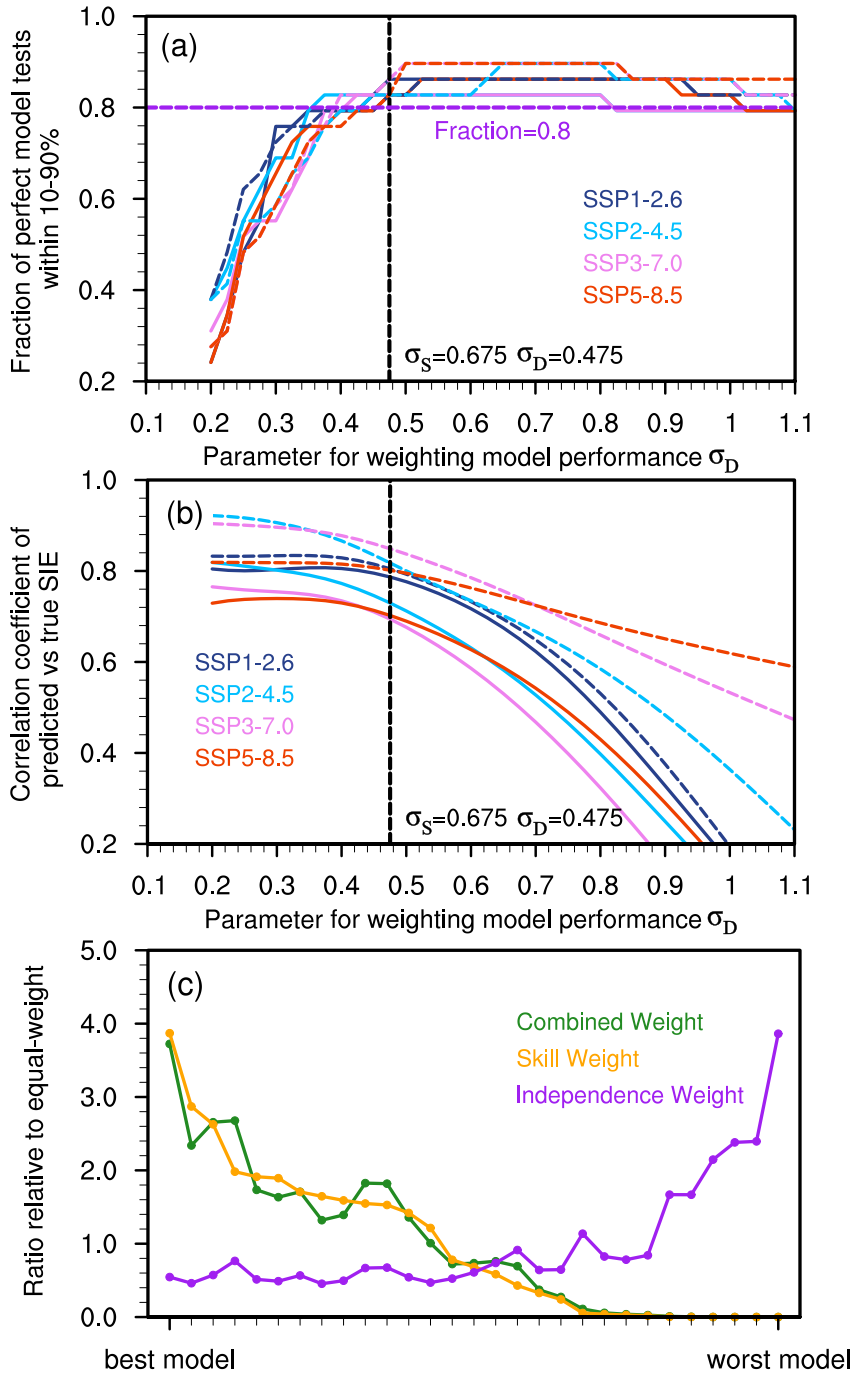

Figure 1. (a) Fraction of cases when the "truth" falls between the 10th and 90th percentiles of the "truth" prediction in the perfect model setup. Arctic sea-ice extent (SIE) changes for the near-term (2021–2050; solid lines) and the long-term (2070–2099; dashed lines) under four emission scenarios (i.e., SSP1-2.6, SSP2-4.5, SSP3-7.0 and SSP5-8.5) are evaluated. The changes are relative to the climatology in 1981–2010 (historical). The vertical dashed line represents the minimum value of σ_D where the fraction exceeds the required 80%. (b) Dependence of correlation coefficients between the predicted and "truth" values of SIE changes on the σ_D in the perfect model setup for the near-term (2021–2050; solid lines) and the long-term (2070–2099; dashed lines) (c) Ratio of the weights (i.e., unequal) of each model estimated by the weighting scheme to an equal-weight; the unequal weights include the skill weight (orange curve), the independence weight (purple curve), and the combined skill–independence weight (green curve).

23284277, 2022, 10, Downloaded from https://agupubs.onlinelibrary.wiley.com/doi/10.1029/2022EF002708 by Universitetsbiblioteket I, Wiley Online Library on [29/12/2022]. See the Terms and Conditions (https://onlinelibrary.wiley.com/terms-and-conditions) on Wiley Online Library for rules of use; OA articles are governed by the applicable Creative Commons License

23284277, 2022, 10, Downloaded from https://agupubs.onlinelibrary.wiley.com/doi/10.1029/2022EF002708 by Universitetsbiblioteket I, Wiley Online Library on [29/12/2022]. See the Terms and Conditions (https://onlinelibrary.wiley.com/terms-and-conditions) on Wiley Online Library for rules of use; OA articles are governed by the applicable Creative Commons License

evaluation in the setup, including SIE changes during 2021–2050 (near-term) and 2070–2099 (long-term) under the SSP1-2.6, SSP2-4.5, SSP3-7.0, and SSP5-8.5 scenarios, respectively. The changes were relative to the climatology of 1981–2010 (historical). Note that there were several pairs of σ_D and σ_s that could ensure the fraction outlined above met the requirement of 80% for all evaluated targets. Since the dependence of the fraction as well as the results of the weighted projections on σ_s were much weaker than their dependence on σ_D (not shown), a value of 0.675 was chosen for σ_s, which points to a minimum value (and hence the strongest weighting) for σ_D of about 0.475 (Figure 1a). In this way, σ_D could be identified properly. Note that if we simply maximized the correlation between the predicted value and the "truth" of the evaluated targets, there would have been an inclination to select a lower σ_D than the proper σ_D value (Figure 1b). We tried to avoid this because Knutti et al. (2017) revealed that values lower than the proper σ_D lead to overconfident results and are therefore likely to produce overly narrow projections. Selection of a larger σ_D than the proper σ_D value may also be inappropriate since such a selection disposes the weighting toward a model democracy such that the model spread may become larger.

3. Results

3.1. Model Weights

Figure 1c shows the distribution of multiple CMIP6 models in terms of the ratio of models' weights to an equal-weight. The independence weight shows an increasing tendency from the best model with the highest skill weight to the worst model with the lowest skill weight (purple curve in Figure 1c). Such a contrary trend between the skill weight and the independence weight reflects the existence of a trade-off phenomenon in the CMIP6 models (orange curve vs. purple curve in Figure 1c). This means that models with better agreement with the observations also tend to have more duplicates. Since the combined skill–independence weight used for sea-ice projections (green curve in Figure 1c) is a product of the skill weight and the independence weight, the above trade-off phenomenon implies that the weighting effect of model skill may offset the weighting effect of model independence. Such an offset may tend to reduce the differences between the projections based on the weighting scheme and those based on a model democracy (Sanderson et al., 2017). The trade-off is relatively strong in CMIP6 owing to the coexistence of model improvement and an increase in the number of participating models. However, such a trade-off problem is effectively overcome by the weighting scheme, as clearly demonstrated by the notable differences in the combined skill–independence weights among individual models (green curve in Figure 1c). With the development of GCMs as well as the increasing number of available GCMs, the trade-off will likely become stronger in future phases of CMIP. Therefore, the weighting scheme may become more important in future research. In addition, high consistency is notable between the distribution of the skill weight and that of the combined skill–independence weight (orange curve vs. green curve in Figure 1c). This means that the models' weights are mainly determined by their performances, which is consistent with the statement made by Knutti et al. (2017) that "*the typical distance to observation is large compared to the distance between duplicate models, and the results are rather insensitive to how strongly model dependence is weighted.*"

3.2. Implementation of the Weighting Scheme

In this section, we evaluate the effect of the weighting scheme on the CMIP6 present-day simulations and the projections compared to the unweighted results. In terms of the RMSE of the climatology and trend, the original outputs of most models have larger RMSE than the unweighted multi-model mean (i.e., the ratio ranges from 1.1 to 4.7; indicated by solid dots in Figures 2a and 2b). This is not the case for the interannual variations (Figure 2c) because averaging multiple models can generally reduce the magnitude of each year's variability in the multi-model mean. Note that the ratio of the RMSE in the unweighted simulations to that in the weighted multi-model mean is even larger (Figures 2a and 2b; indicated by the circles), which demonstrates that the weighting scheme efficiently reduces the bias. The RMSE of the climatology and interannual variability of SAT in the weighted multi-model mean is about 0.6 and 0.9 times that in the unweighted multi-model mean (blue crosses in the middle column of Figures 2a and 2c). In addition, the pattern correlations of the trend and interannual variability of SAT in the weighted multi-model mean are approximately 0.15 and 0.2 higher than those in the unweighted multi-model mean (blue vs. black crosses in the middle column of Figures 2e and 2f). The weighting scheme also constrains the biases in the simulations of present-day SIC and SST; however, the magnitude of bias

10.1029/2022EF002708

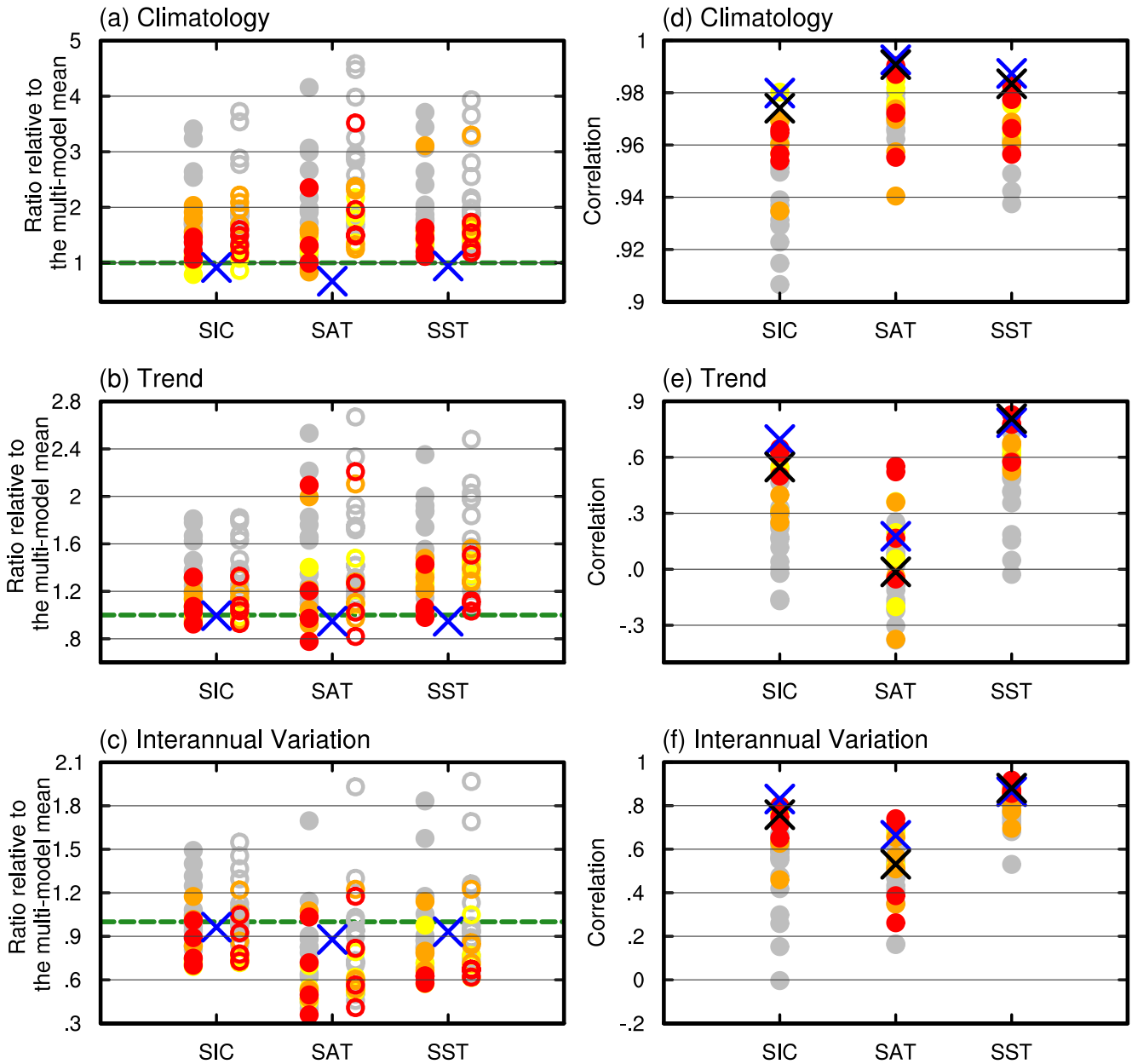

Figure 2. Summary of the (a–c) biases and (d–f) spatial patterns of the weighted and unweighted simulations compared with their observational counterparts during 1980–2014. (a–c) Ratio between each model's root-mean-square error (RMSE) (simulation vs. observation) and the multi-model mean's RMSE for the (a) climatology, (b) trend, and (c) interannual variation of September Arctic (60°–90°N) sea ice concentration (SIC), surface air temperature (SAT), and sea surface temperature (SST). Each solid dot/circle represents a ratio between the unweighted individual model's RMSE and the unweighted/weighted multi-model mean's RMSE; the blue crosses indicate the ratio between the weighted multi-model mean's RMSE and the unweighted multi-model mean's RMSE. The green dashed horizontal lines indicate the value of 1.0. (d–f) Pattern correlation of the climatology, trend and interannual variation for the September Arctic SIC, SAT, and SST between simulation and observation. Each dot indicates the pattern correlation between the unweighted individual models and the observation, and the blue/black crosses indicate the pattern correlation between the weighted/unweighted multi-model mean and the observation. The red, orange and yellow dots or circles indicate the models that get the 1st–4th, 5th–8th, and 9th–12th largest weights, respectively; and the gray dots/circles indicate the remaining models.

reduction is smaller than that of the bias reduction for SAT. This is unsurprising because the original outputs of the CMIP6 models capture the present-day Arctic sea-ice variability well (Notz & SIMIP Community, 2020).

To test whether the weighting scheme can constrain the uncertainty in SIE projections, we illustrate in Figure 3a the range of multiple models' September SIE in the three specific 30-year periods. The ranges are compared between the unweighted (i.e., equal weighting) and weighted (i.e., by the weighting scheme) models. Given that

23284277, 2022, 10, Downloaded from https://agupubs.onlinelibrary.wiley.com/doi/10.1029/2022EF002708 by Universitetsbiblioteket I, Wiley Online Library on [29/12/2022]. See the Terms and Conditions (https://onlinelibrary.wiley.com/terms-and-conditions) on Wiley Online Library for rules of use; OA articles are governed by the applicable Creative Commons License

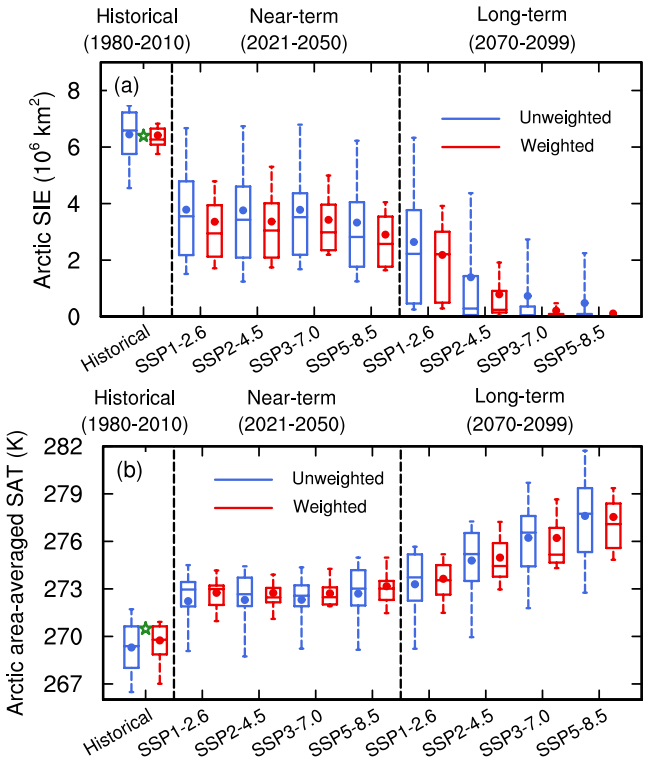

Figure 3. Statistical distribution of September Arctic climate within weighted (red) and unweighted (blue) multiple models: (a) climatological Arctic sea-ice extent and (b) climatological Arctic area-averaged surface air temperature in the historical (1981–2010), near-term (2021–2050) and long-term (2070–2099) periods under the SSP1-2.6, SSP2-4.5, SSP3-7.0, and SSP5-8.5 scenarios. The whiskers indicate the 10th and 90th percentiles; the box indicates the 25th and 75th percentiles; and the line inside the box indicates the 50th percentile. Dots indicate the multi-model mean and green stars indicate observations.

the long-term Arctic sea-ice variability simulated by GCMs is linearly related to Arctic warming (Bonan, Schneider, et al., 2021; Jahn, 2018; Rosenblum & Eisenman, 2017), we also show the range of multiple models' Arctic area-averaged SAT based on the two approaches (Figure 3b). It is notable that both the SIE and SAT refined by the weighting scheme have smaller spread relative to those based on model democracy, which is the case for both historical simulations and future projections. Additionally, compared to observations (green star in Figure 3b), the unweighted multi-model mean underestimates the climatology of Arctic SAT by 1.22 K (blue dot in Figure 3b). This underestimation may reflect the sensitivity of the climate system in climate models to a given amount of anthropogenic CO_2 emissions, which implies that the unweighted multi-model mean may also underestimate the future Arctic warming, especially under high-emissions scenarios (i.e., SSP3-7.0 and SSP5-8.5). The weighted multi-model mean reduces this bias in the historical simulations of climatological Arctic SAT and projects a stronger warming under all pathway scenarios (red dots in Figure 3b). As a result, despite the fact that the unweighted and weighted multi-model means show a similar historical SIE climatology, the weighted multi-model mean projects evidently less SIE in the future (red dots in Figure 3a), indicating a faster tendency to an ice-free Arctic in September than the one originally projected by climate models. At the end of this century, the weighted multiple models project there to be almost no remaining sea ice in the Arctic under the two high-emissions scenarios (i.e., SSP3-7.0 and SSP5-8.5) (Figure 3a; red dots). This indicates that the first year of an ice-free Arctic will very likely occur before 2100 unless emissions of greenhouse gases are largely reduced.

3.3. Projections of the Timing of an Ice-Free Arctic in September

Figure 4 illustrates the projections of September SIE and the first year of an ice-free Arctic derived by the model democracy and the weighting scheme. Due to considerable improvements in sea-ice simulations in CMIP6 relative to previous phases of CMIP, the time series of SIE simulated by the mean of the weighted CMIP6 models has much less bias with respect to observations when compared to the mean of weighted CMIP3 and CMIP5 models [see red curve in Figure 1c of Knutti et al. (2017)]. It is notable that simulations based on the weighted CMIP6 models capture the observed decline in September Arctic SIE well, and such a performance provides more confidence that the weighting scheme can obtain reliable projections of the timing of an ice-free Arctic. The weighted multi-model mean (solid colored curves in Figures 4a–4d) projects a more rapid decrease in Arctic SIE than the unweighted multi-model mean (solid black curves in Figures 4a–4d), indicating an earlier occurrence of the first year of an ice-free Arctic than the raw projections under the SSP2-4.5, SSP3-3.7, and SSP5-8.5 scenarios. In addition, the large spread of projected SIE among the original outputs of the CMIP6 models (gray bands in Figures 4a–4d) is efficiently reduced by the weighting scheme (colored bands in Figures 4a–4d). The spread among the weighted/unweighted models indicates 2040–2072/2039 to the next century and 2038–2071/2037–2097 as the period in which the first year of an ice-free Arctic is likely to occur under the SSP3-7.0 and SSP5-8.5 scenarios, respectively (Figures 4c and 4d). Comparison between the spread among the weighted and unweighted models indicates that using the weighting scheme may reduce the spread of the projected first year of an ice-free Arctic by about 29 and 27 years under the SSP3-7.0 and SSP5-8.5 scenarios, respectively. Comparatively, under a relatively lower-emissions scenario (i.e., SSP1-2.6), the spread among both the weighted and unweighted models remains mostly above the threshold of ice-free conditions, indicating the need to efficiently slow global warming to prevent an ice-free Arctic from occurring this century. Figure 4e quantitatively illustrates the effect of the weighting scheme on the projections of the first year of an ice-free Arctic. Under higher-emissions scenarios, the Arctic is projected to become ice free earlier over the coming decades. Interestingly, without being weighted, most models under the SSP2-4.5, SSP3-7.0, and SSP5-8.5 scenarios project an ice-free Arctic before 2100, and the timing in most models is even earlier (see dots in Figure 4e) than in the multi-model mean (black crosses

23284277, 2022, 10, Downloaded from https://agupubs.onlinelibrary.wiley.com/doi/10.1029/2022EF002708 by Universitetsbiblioteket I, Wiley Online Library on [29/12/2022]. See the Terms and Conditions (https://onlinelibrary.wiley.com/terms-and-conditions) on Wiley Online Library for rules of use; OA articles are governed by the applicable Creative Commons License

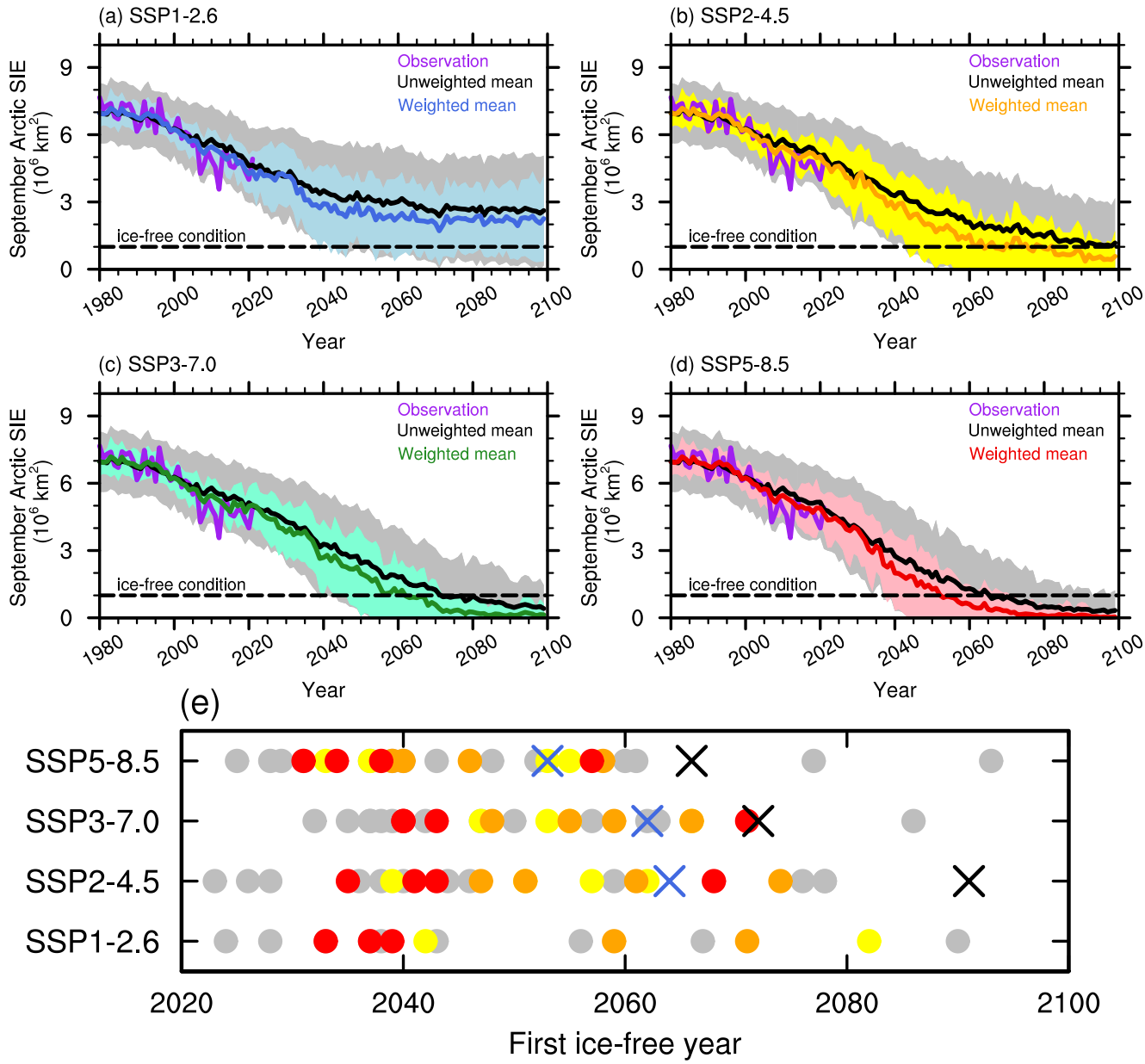

Figure 4. (a–d) Time series of September Arctic sea-ice extent (SIE) in the weighted and unweighted multi-model projections under the SSP1-2.6, SSP2-4.5, SSP3-7.0, and SSP5-8.5 scenarios. The colored curves and bands indicate the weighted multi-model mean and spread, respectively. The black curves and gray bands indicate the unweighted multi-model mean and spread, respectively. The purple solid curves represent observations. A value of Arctic SIE of 1×10^6 km^2 is defined as the threshold for an ice-free condition (horizontal dashed lines). (e) First year of an ice-free Arctic in September under the SSP1-2.6, SSP2-4.5, SSP3-7.0, and SSP5-8.5 scenarios, in which dots indicate the unweighted individual models; the red, orange and yellow dots indicate models that achieve the 1st–4th, 5th–8th, and 9th–12th largest weights, respectively; and the gray dots indicate the remaining models. Blue and black crosses represent the weighted and unweighted multi-model means, respectively.

in Figure 4e). This is because a few individual models dramatically underestimate the rate of Arctic sea-ice decline (see Figures 3b and 3c in Wang et al. (2021)), which can strongly affect the projection of the unweighted multi-model mean, thereby further emphasizing the importance of applying the weighting scheme. Under the SSP2-4.5, SSP3-7.0 and SSP5-8.5 scenarios, the weighted (unweighted) multi-model mean projects that the first year of an ice-free Arctic is likely to occur in 2064, 2062, and 2053 (2091, 2072, and 2066), respectively (crosses in Figure 4e). In other words, with the uncertainties constrained, the CMIP6 models project a plausible faster decline approaching an ice-free Arctic about 27, 10, and 13 years earlier under the three scenarios, respectively, than that indicated by the unconstrained projections. By comparison, under the sustainable development scenario (i.e., SSP1-2.6), both the weighted and unweighted multi-model means project that an ice-free Arctic

23284277, 2022, 10, Downloaded from https://agupubs.onlinelibrary.wiley.com/doi/10.1029/2022EF002708 by Universitetsbiblioteket I, Wiley Online Library on [29/12/2022]. See the Terms and Conditions (https://onlinelibrary.wiley.com/terms-and-conditions) on Wiley Online Library for rules of use; OA articles are governed by the applicable Creative Commons License

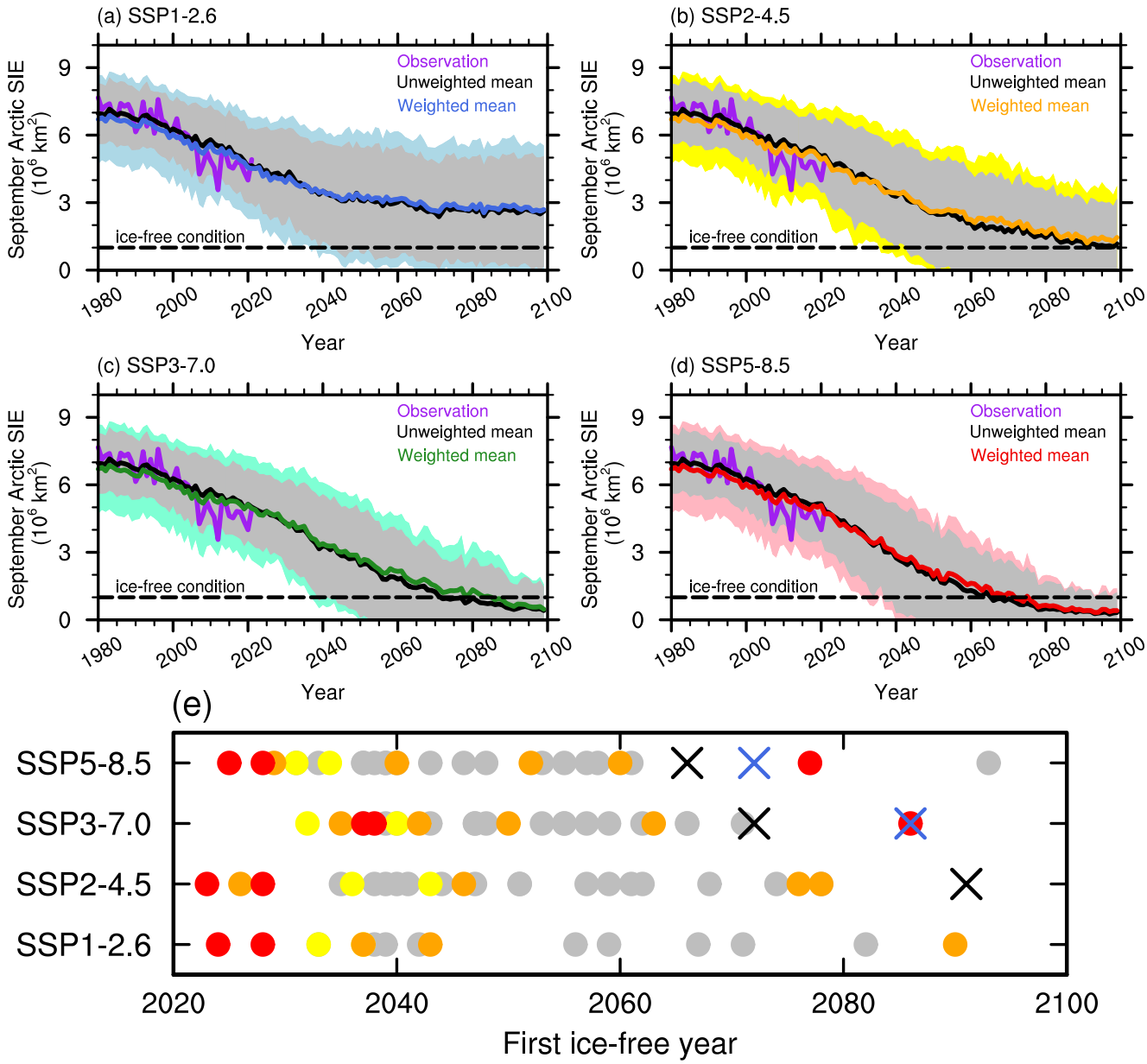

Figure 5. As in Figure 4 but with the weighting scheme only considering the model independence.

may not occur in this century. The above results indicate that the first year of an ice-free Arctic is somewhat sensitive to the emissions scenario considered, which can be attributed to the evident scenario dependence in the long-term future time evolution of Arctic sea ice during the second half of the 21st century (Notz & SIMIP Community, 2020). Meanwhile, the results seem to be somewhat different from those reported in DeRepentigny et al. (2020) derived from two configurations of CESM2, who suggested that the timing of the first ice-free conditions in summer is insensitive to the choice of CMIP6 future emissions scenario. A possible reason is that our results are derived from multiple models from CMIP6, whereas DeRepentigny et al. (2020) based their findings on the results of a single model. Actually, several individual CMIP6 models project that an ice-free Arctic summer is likely to occur under all the scenarios considered in this study (Figure 4e), which includes the possible conclusions drawn from one single model (DeRepentigny et al., 2020).

Given the development and increasing number of state-of-the-art GCMs participating in CMIP6, we further investigate the effect of model interdependence on the Arctic sea-ice projections. Figure 5 shows the

23284277, 2022, 10, Downloaded from https://agupubs.onlinelibrary.wiley.com/doi/10.1029/2022EF002708 by Universitetsbiblioteket I, Wiley Online Library on [29/12/2022]. See the Terms and Conditions (https://onlinelibrary.wiley.com/terms-and-conditions) on Wiley Online Library for rules of use; OA articles are governed by the applicable Creative Commons License

23284277, 2022, 10, Downloaded from https://agupubs.onlinelibrary.wiley.com/doi/10.1029/2022EF002708 by Universitetsbiblioteket I, Wiley Online Library on [29/12/2022]. See the Terms and Conditions (https://onlinelibrary.wiley.com/terms-and-conditions) on Wiley Online Library for rules of use; OA articles are governed by the applicable Creative Commons License

independence-weighted and unweighted CMIP6 projections of September Arctic SIE as well as the first year of an ice-free Arctic. It turns out that when CMIP6 models are solely weighted based on their independence, the multi-model spread (colored bands in Figures 5a–5d) becomes even larger than the spread among the unweighted models (gray band in Figures 5a–5d), leading to increased uncertainty. Such a spread change indicates that there is duplicate information in the CMIP6 GCM outputs which may affect the projections. The impacts of these duplicate information, however, cannot be taken into account by the prevailing model democracy. In addition, the increase in multi-model spread implies that some CMIP6 models that have stronger independence (assigned with larger independence weights) may have lower simulation and projection skill, suggesting that both model independence and skill should be taken into account. These results are consistent with the conclusions drawn by a recent study that redundant information provided by similar models will lead to underestimation of the projection uncertainty (Merrifield et al., 2019). Comparison between the weighted and unweighted projections shown in Figure 4a–4d and 5a–5d indicates that considering model skill plays a central role in constraining the uncertainty of Arctic SIE projections. Figure 5e quantitatively illustrates the effect of model interdependence on the projections of the first year of an ice-free Arctic. Consistent with the results shown in Figures 5a–5d, the independence-weighted multi-model mean (colored crosses in Figure 5e) projects an even later occurrence of an ice-free Arctic than the unweighted multi-model mean (black crosses in Figure 5e). This means that models with a lower rate of sea-ice decline are assigned larger independence weights. Overall, solely considering model independence is still impractical in seeking to provide more reliable projections of Arctic sea ice.

4. Discussion

4.1. Choice of Diagnostics for Weighted Projections

Previous studies have suggested that the robustness of results derived by a weighting scheme needs to be tested to maximize their comparability across studies (Brunner et al., 2020; Knutti et al., 2017; Lorenz et al., 2018). If the results are obviously sensitive to the choice of metrics for the weight estimation, the weighting scheme may be too aggressive (i.e., overfitting). Here, we tested the robustness of the weighted projections in this study through adopting a certain range of choices in the diagnostic variables. Four choices were produced based on the consideration of (a) SIE, (b) SIE + SIC, (c) SIE + SLP, and (d) SIE + SIC + SLP in the weight estimation (more details can be found in Section 2.6). The weighted projections of September SIE corresponding to each choice are shown in Figure 6. Among different choices of diagnostic variables used for the weight estimation, inclusion of all three variables (SIE + SIC + SLP) leads to the minimum spread (light blue band in Figure 6) of multiple models under all emission scenarios. In addition, the first year of an ice-free Arctic indicated by the weighted multi-model mean based on the inclusion of SIE + SIC/SIE + SLP is a bit later/earlier than that derived from the diagnostics of SIE + SIC + SLP (see red and green curves compared to the blue curve in Figure 6). As shown in Figure 7, compared to the multi-model mean weighted by SIE (Figure 7a) or SIE + SIC (Figure 7b), the multi-model mean weighted by SIE + SLP (Figure 7c), or SIE + SIC + SLP (Figure 7d), projects an earlier occurrence of an ice-free Arctic under the SSP2-4.5, SSP3-7.0, and SSP5-8.5 scenarios. However, despite the abovementioned differences, it is notable that the different choices of diagnostic variables lead to robust and obvious reductions in the projection uncertainty of Arctic SIE (i.e., the range of the colored bands is much smaller than that of the gray band in Figure 6). In terms of the occurrence of an ice-free Arctic, the multi-model mean weighted by different diagnostic variables consistently indicates that it is unlikely to occur before the end of the 21st century under the sustainable development scenario (i.e., SSP1-2.6). Therefore, despite the abovementioned slight differences among the projections constrained by different diagnostic variables, we conclude that the results derived from the weighting scheme in this study are reasonably robust and comparable with results shown in previous studies.

4.2. Impact of Internal Variability

Previous studies have indicated that internal climate variability may affect the Arctic sea-ice variability and can increase the uncertainty in sea-ice projections (DeRepentigny et al., 2020; Ding et al., 2017, 2019). To investigate the potential effect of internal variability on the results derived from the weighting scheme in this study, we further employed a 50-member single-model initial condition large ensemble (SMILE), the CESM2-LE (see Section 2.2). The 50-member ensemble and the 29 CMIP6 models are used in two ways to construct two different categories of large ensembles:

10.1029/2022EF002708

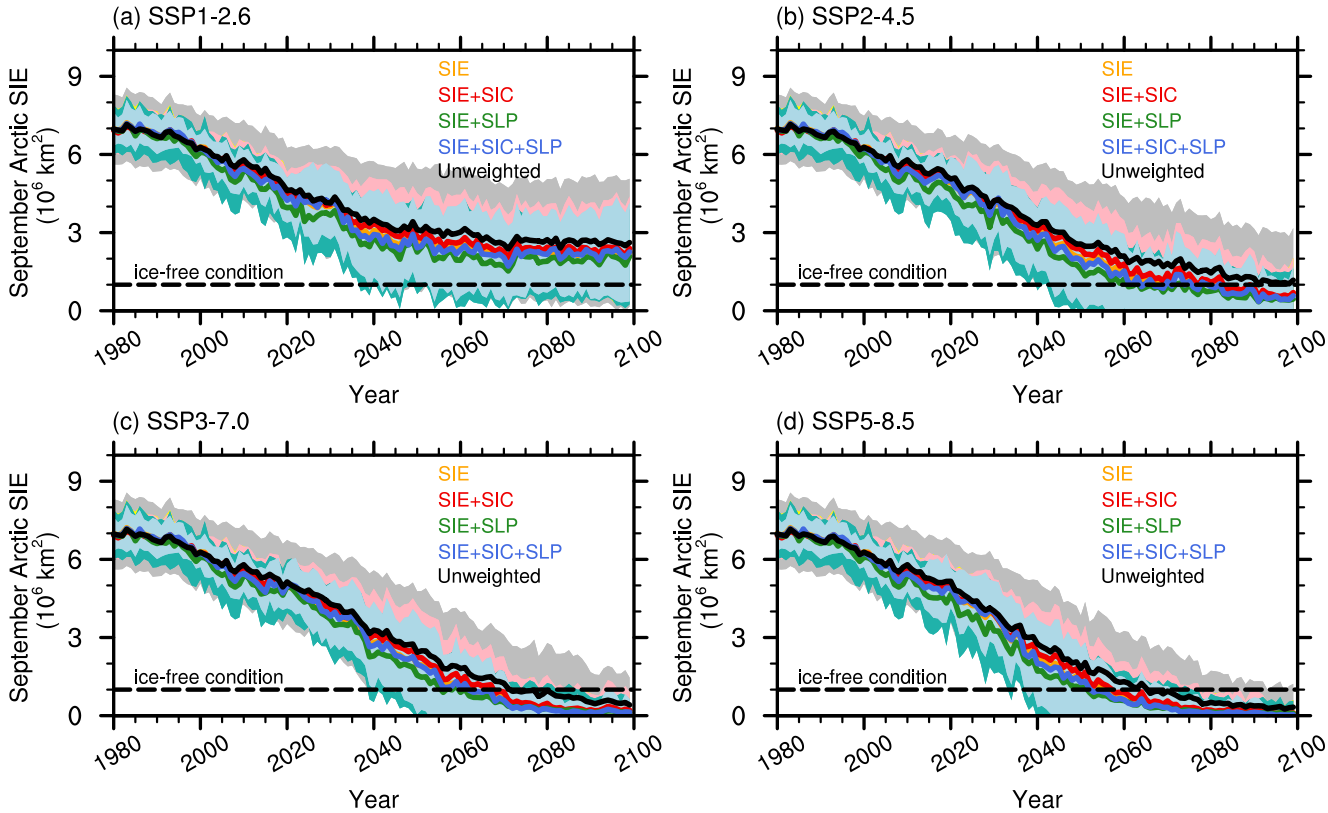

Figure 6. Projections of September Arctic sea-ice extent (SIE) under the SSP1-2.6, SSP2-4.5, SSP3-7.0, and SSP5-8.5 scenarios constrained by different choices of diagnostic variables: SIE (orange); SIE + SIC (red); SIE + SLP (green); SIE + SIC + SLP (blue). The colored curves and bands indicate the weighted multi-model mean and spread, respectively. The black curves and gray bands indicate the unweighted multi-model mean and spread, respectively. A value of Arctic SIE of 1×10^6 km^2 is defined as the threshold for an ice-free condition (horizontal dashed lines).

1. A large ensemble containing 29 CMIP6 models and the first ensemble member of the 50-member CESM2-LE, which gave a total amount of 30 members. Such a scheme is used to investigate the model uncertainty.
2. A large ensemble that included 29 CMIP6 models and all 50 ensemble members of the 50-member CESM2-LE, which gave a total amount of 79 members. Such a scheme can be seen as representing the superposition of internal variability on model uncertainty.

The weighting scheme was separately applied to the two large ensembles. Note that the weighting based on the two ensembles shared the same pair of shape parameters, σ_D and σ_s, following Merrifield et al. (2019). Their values were determined by a perfect model setup. The perfect model setup was implemented using the 29 CMIP6 models and the first ensemble member from the 50-member CESM2-LE (i.e., the first large-ensemble scheme outlined above). That was because the redundant information provided by similar members of CESM2-LE would bias the perfect model setup (Merrifield et al., 2019). Weighting based on the second large-ensemble scheme, which contained considerably similar members from CESM2-LE, indicated the need to appropriately select a σ_s that was large enough for similar members from CESM2-LE could be considered as redundant members, but not so large that most CMIP6 models were considered as redundant. Here, σ_s was determined as two standard deviations below the mean CESM2-LE member-to-member distances S_{ij} of 0.75, following Merrifield et al. (2019). The σ_s value pointed to a value for σ_D of 0.475 according to the perfect model setup (not shown).

Figure 8 shows the multi-model projections of September SIE derived by weighting the two categories of large ensembles (green curves and green bands). For comparison, the unweighted projections based on the two ensembles are also shown (black curves and gray bands in Figure 8). The unweighted multi-model mean of the first large ensemble (black curve in Figure 8a) projects a slower decline of SIE relative to that projected by the unweighted multi-model mean of the second large ensemble (black curve in Figure 8b). The spread of projected SIE among the multiple unweighted members of the first large ensemble (gray band in Figure 8a) is larger than that of the

23284277, 2022, 10, Downloaded from https://agupubs.onlinelibrary.wiley.com/doi/10.1029/2022EF002708 by Universitetsbiblioteket I, Wiley Online Library on [29/12/2022]. See the Terms and Conditions (https://onlinelibrary.wiley.com/terms-and-conditions) on Wiley Online Library for rules of use; OA articles are governed by the applicable Creative Commons License

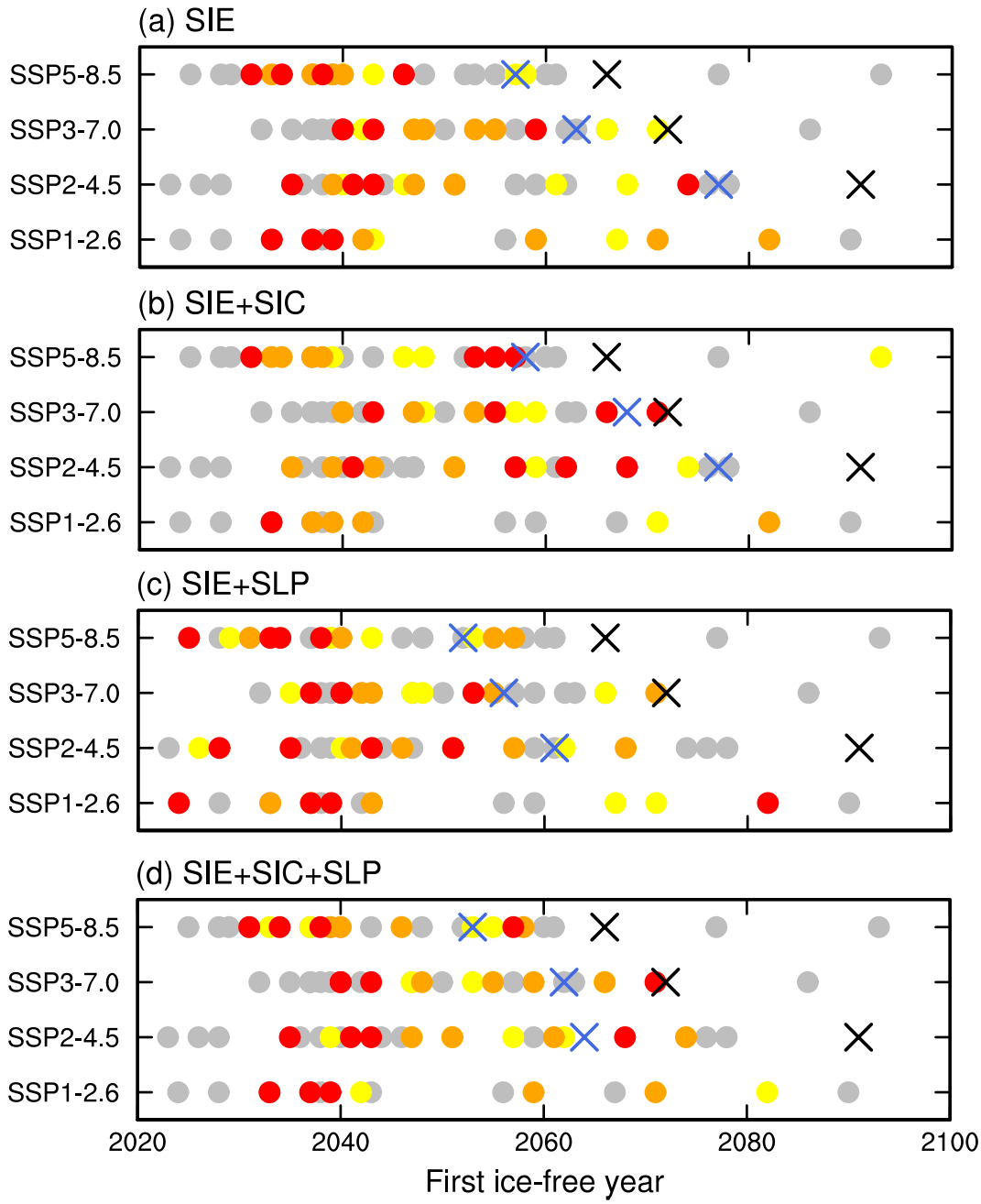

Figure 7. First year of an ice-free Arctic in September as indicated by the weighted and unweighted multi-model projections under the SSP1-2.6, SSP2-4.5, SSP3-7.0, and SSP5-8.5 scenarios derived from different choices of diagnostic variables: (a) sea-ice extent (SIE); (b) SIE + SIC; (c) SIE + SLP; and (d) SIE + SIC + SLP. Dots indicate the unweighted individual models (same as in Figures 4e and 5e). Blue/black crosses represent the weighted/unweighted multi-model mean. The red, orange and yellow dots indicate the models that achieve the 1st–4th, 5th–8th, and 9th–12th largest weights, respectively; and the gray dots indicate the remaining models.

second large ensemble (gray band in Figure 8b) before 1990 and after 2020. This indicates that adding considerably similar members to large-ensemble models will affect the multi-model mean and may lead to unreasonable reductions in projection uncertainty from the original outputs of climate models. This is consistent with the conclusion drawn by Merrifield et al. (2019) that redundant information from the SMILE results in an underestimation of uncertainty. Different from the unweighted multi-model projections, the weighted multi-model mean of the two large ensembles indicates similar trends of SIE in the future (green curves in Figure 8). In addition,

23284277, 2022, 10, Downloaded from https://agupubs.onlinelibrary.wiley.com/doi/10.1029/2022EF002708 by Universitetsbiblioteket I, Wiley Online Library on [29/12/2022]. See the Terms and Conditions (https://onlinelibrary.wiley.com/terms-and-conditions) on Wiley Online Library for rules of use; OA articles are governed by the applicable Creative Commons License

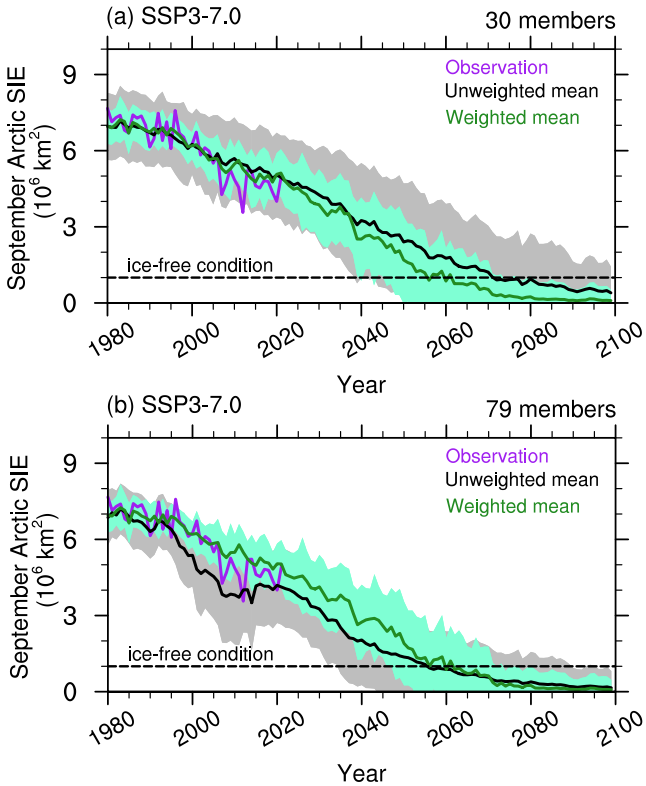

Figure 8. Time series of September Arctic sea-ice extent (SIE) from the weighted and unweighted multi-model projections under the SSP3-7.0 scenario based on the (a) first and (b) second large-ensemble category (outlined in Section 4.2). The green curves and bands indicate the weighted multi-model mean and spread, respectively. The black curves and gray bands indicate the unweighted multi-model mean and spread, respectively. The purple solid curves represent observations. A value of Arctic SIE of 1×10^6 km^2 is defined as the threshold for an ice-free condition (horizontal dashed lines).

the spread of projected SIE among the weighted multiple members of the two large ensembles is also similar (green bands in Figure 8). In summary, despite the fact that internal variability strongly affects the multi-model mean and spread of projections from the original outputs of climate models, it has a negligible impact on projections derived from the weighting scheme in this study.

5. Summary and Conclusions

Numerous studies have indicated that dramatic Arctic sea-ice decline will lead to a possible ice-free Arctic in summer by the end of this century (Bonan, Schneider, et al., 2021; IPCC, 2021; Jahn, 2018; Laliberté et al., 2016; Sigmond et al., 2018). However, the projection of an ice-free Arctic summer based on climate models intrinsically carries large uncertainty arising primarily from internal variability and the different structures of climate models (Bonan, Lehner, & Holland, 2021). This uncertainty has not been well understood so far, and may not be appropriately estimated by simple and traditional methods that regard models as equally important despite their different performances and considerable interdependence. With the development and increase in the number of state-of-the-art climate models, it is becoming more necessary to consider both the skill and independence of models so as to provide more convincing projections.

In this study, through applying a weighting scheme proposed in Knutti et al. (2017), we show that the large uncertainties in CMIP6 projections of the timing of an ice-free Arctic summer can be efficiently constrained by weighting both the skill and independence of multi-model simulations. We found that biases in the CMIP6 simulations of SIC, SST and especially the SAT around the Arctic region, relative to observations, can be efficiently reduced by the weighting scheme. The bias-constrained present-day simulations increase the level of confidence in the sea-ice projections derived from the weighting scheme. The weighted projections indicate a faster tendency to an ice-free Arctic in this century than the unweighted projections. The spread among the weighted models, which is largely narrowed by the weighting scheme, indicates that the first year of an ice-free Arctic is likely to occur during 2040–2072 (~2062 in the weighted multi-model mean) and 2038–2071 (~2053 in the weighted multi-model mean) under the SSP3-7.0 and SSP5-8.5 scenarios, respectively. More specifically, the weighting scheme reduces the spread of the projected first year of an ice-free Arctic by about 29 and 27 years under the SSP3-7.0 and SSP5-8.5 scenarios, respectively. Under the intermediate emissions scenario (i.e., SSP2-4.5), the weighted multi-model mean projects that the first year of an ice-free Arctic is likely to occur a bit later (2064). Notably, after the constraint of uncertainty by the weighting scheme, CMIP6 models project that an ice-free Arctic seems to be inevitable this century under the SSP2-4.5 scenario, but may not occur before 2100 under the SSP1-2.6 scenario.

Given the dramatic increase in the number of GCMs in CMIP6 compared with previous phases of CMIP, we further investigated the sole effect of model interdependence on the CMIP6 projections of September Arctic SIE. We found that, when models that have stronger independence are assigned with larger weights by the weighting scheme, the spread of the projected Arctic SIE among the multiple models becomes slightly larger than that of the original unweighted projections. This indicates that the independent models in the CMIP6 archive show relatively poor skill, reflecting the trade-off phenomenon detailed in Sanderson et al. (2017). The trade-off phenomenon implies that the weighting effect of model skill may offset the weighting effect of model independence, which will reduce the differences between the projections based on the weighting scheme and those based on a model democracy. Satisfactorily, it is shown in this study that such a trade-off problem is effectively overcome by the weighting scheme. Furthermore, this also emphasizes the importance of considering both model skill and independence in the weighting scheme, which, by doing so, can better constrain the uncertainty in climate model projections.

23284277, 2022, 10, Downloaded from https://agupubs.onlinelibrary.wiley.com/doi/10.1029/2022EF002708 by Universitetsbiblioteket I, Wiley Online Library on [29/12/2022]. See the Terms and Conditions (https://onlinelibrary.wiley.com/terms-and-conditions) on Wiley Online Library for rules of use; OA articles are governed by the applicable Creative Commons License

Conflict of Interest

The authors declare no conflicts of interest relevant to this study.

Data Availability Statement

All the data analyzed in this study are openly available. The monthly mean sea-ice concentration is from the Met Office's Hadley Centre Sea Ice and Sea Surface Temperature data set at https://www.metoffice.gov.uk/hadobs/hadisst/data/download.html. Users should click on the link named "HadISST_ice.nc.gz" to download the compressed nc file. The ERA5 reanalysis data used in this study can be retrieved from the data portal at https://cds.climate.copernicus.eu/cdsapp#!/dataset/reanalysis-era5-single-levels-monthly-means?tab=form. The monthly Arctic sea-ice extent and sea-ice area are from the NSIDC Sea Ice Index at https://nsidc.org/data/G02135/versions/3. CMIP6 simulations provided by ESGF can be found via the following open-source link: https://esgf-node.llnl.gov/search/cmip6/. Users should select the *Variable* as *siconc*, *tas*, *tos* and *psl*, which stand for sea-ice concentration, surface air temperature, sea surface temperature, and sea level pressure, respectively. Select the *Frequency* as *mon*; select the Table ID as *Amon*, *Omon*, and *Simon*; select the *Experiment ID* as historical, ssp126, ssp245, ssp370, and ssp585; select the CMIP6 models employed in this study (see Table 1); and then download the nc files that appear as the search outputs. The CESM2-LE simulations can be accessed via the following open-source link: https://www.cesm.ucar.edu/projects/community-projects/LENS2/data-sets.html. Users should select the *Monthly* simulation data for *Atmosphere* components and click on the links named "ucar.cgd.cesm2le.atm.proc.monthly_ave.ICEFRAC" and "ucar.cgd.cesm2le.atm.proc.monthly_ave.PSL" to download the nc files for sea-ice concentration and sea level pressure, respectively.

Acknowledgments
This research was supported by the National Natural Science Foundation of China (42088101, 42075030). He SP was supported by a Research Council of Norway project (BASIC, Grant 325440).

References

Årthun, M., Onarheim, I. H., Dörr, J., & Eldevik, T. (2021). The seasonal and regional transition to an ice-free Arctic. *Geophysical Research Letters*, *48*(1), e2020GL090825. https://doi.org/10.1029/2020gl090825

Alekseev, G. V., Glok, N. I., Vyazilova, A. E., Kharlanenkova, N. E., & Kulakov, M. Y. (2021). Influence of SST in low latitudes on the Arctic warming and sea ice. *Journal of Marine Science and Engineering*, *9*(10), 1145. https://doi.org/10.3390/jmse9101145

Boé, J., Hall, A., & Qu, X. (2009). September sea-ice cover in the Arctic Ocean projected to vanish by 2100. *Nature Geoscience*, *2*(5), 341–343. https://doi.org/10.1038/ngeo467

Bonan, D. B., Lehner, F., & Holland, M. M. (2021). Partitioning uncertainty in projections of Arctic sea ice. *Environmental Research Letters*, *16*(4), 044002. https://doi.org/10.1088/1748-9326/abe0ec

Bonan, D. B., Schneider, T., Eisenman, I., & Wills, R. C. J. (2021). Constraining the date of a seasonally ice-free Arctic using a simple model. *Geophysical Research Letters*, *48*(18), e2021GL094309. https://doi.org/10.1029/2021gl094309

Brunner, L., Pendergrass, A. G., Lehner, F., Merrifield, A. L., Lorenz, R., & Knutti, R. (2020). Reduced global warming from CMIP6 projections when weighting models by performance and independence. *Earth System Dynamics*, *11*(4), 995–1012. https://doi.org/10.5194/esd-11-995-2020

Cohen, J., Screen, J. A., Furtado, J. C., Barlow, M., Whittleston, D., Coumou, D., et al. (2014). Recent Arctic amplification and extreme mid-latitude weather. *Nature Geoscience*, *7*(9), 627–637. https://doi.org/10.1038/ngeo2234

Cohen, J., Zhang, X., Francis, J., Jung, T., Kwok, R., Overland, J., et al. (2020). Divergent consensuses on Arctic amplification influence on midlatitude severe winter weather. *Nature Climate Change*, *10*(1), 20–29. https://doi.org/10.1038/s41558-019-0662-y

Danabasoglu, G., Lamarque, J.-F., Bacmeister, J., Bailey, D. A., DuVivier, A. K., Edwards, J., et al. (2020). The Community Earth System Model Version 2 (CESM2). *Journal of Advances in Modeling Earth Systems*, *12*, e2019MS001916. https://doi.org/10.1029/2019ms001916

DeRepentigny, P., Jahn, A., Holland, M. M., Kay, J. E., Fasullo, J., Lamarque, J. F., et al. (2022). Enhanced simulated early 21st century Arctic sea ice loss due to CMIP6 biomass burning emissions. *Science Advances*, *8*(30), eabo2405. https://doi.org/10.1126/sciadv.abo2405

DeRepentigny, P., Jahn, A., Holland, M. M., & Smith, A. (2020). Arctic sea ice in two configurations of the CESM2 during the 20th and 21st centuries. *Journal of Geophysical Research: Oceans*, *125*(9), e2020JC016133. https://doi.org/10.1029/2020jc016133

Diebold, F. X., & Rudebusch, G. D. (2021). Probability assessments of an ice-free Arctic: Comparing statistical and climate model projections. *Journal of Econometrics*. https://doi.org/10.1016/j.jeconom.2020.12.007

Ding, Q., Schweiger, A., L'Heureux, M., Battisti, D., Po-Chedley, S., Johnson, N., et al. (2017). Influence of high-latitude atmospheric circulation changes on summertime Arctic sea ice. *Nature Climate Change*, *7*(4), 289–295. https://doi.org/10.1038/nclimate3241

Ding, Q., Schweiger, A., L'Heureux, M., Steig, E. J., Battisti, D. S., Johnson, N. C., et al. (2019). Fingerprints of internal drivers of Arctic sea ice loss in observations and model simulations. *Nature Geoscience*, *12*(1), 28–33. https://doi.org/10.1038/s41561-018-0256-8

Docquier, D., & Koenigk, T. (2021). Observation-based selection of climate models projects Arctic ice-free summers around 2035. *Communications Earth Environment*, *2*(1), 144. https://doi.org/10.1038/s43247-021-00214-7

Eyring, V., Bony, S., Meehl, G. A., Senior, C. A., Stevens, B., Stouffer, R. J., & Taylor, K. E. (2016). Overview of the Coupled Model Intercomparison Project Phase 6 (CMIP6) experimental design and organization. *Geoscientific Model Development*, *9*(5), 1937–1958. https://doi.org/10.5194/gmd-9-1937-2016

Fetterer, F., Knowles, K., Meier, W. N., Savoie, M., & Windnagel, A. K. (2017). *Sea Ice Index, Version 3* [Dataset]. NSIDC: National Snow and Ice Data Center. https://doi.org/10.7265/N5K072F8

Francis, J. A., & Vavrus, S. J. (2012). Evidence linking Arctic amplification to extreme weather in mid-latitudes. *Geophysical Research Letters*, *39*(6), L06801. https://doi.org/10.1029/2012gl051000

Guo, H., Bao, A., Chen, T., Zheng, G., Wang, Y., Jiang, L., & De Maeyer, P. (2021). Assessment of CMIP6 in simulating precipitation over arid Central Asia. *Atmospheric Research*, *252*, 105451. https://doi.org/10.1016/j.atmosres.2021.105451

23284277, 2022, 10, Downloaded from https://agupubs.onlinelibrary.wiley.com/doi/10.1029/2022EF002708 by Universitetsbiblioteket I, Wiley Online Library on [29/12/2022]. See the Terms and Conditions (https://onlinelibrary.wiley.com/terms-and-conditions) on Wiley Online Library for rules of use; OA articles are governed by the applicable Creative Commons License

Herger, N., Abramowitz, G., Knutti, R., Angélil, O., Lehmann, K., & Sanderson, B. M. (2018). Selecting a climate model subset to optimise key ensemble properties. *Earth System Dynamics*, *9*(1), 135–151. https://doi.org/10.5194/esd-9-135-2018

Hersbach, H., Bell, B., Berrisford, P., Hirahara, S., Horanyi, A., Munoz-Sabater, J., et al. (2020). The ERA5 global reanalysis. *Quarterly Journal of the Royal Meteorological Society*, *146*(730), 1999–2049. https://doi.org/10.1002/qj.3803

IPCC. (2013). Contribution of working group I to the fifth assessment report of the intergovernmental Panel on climate change. In T. F., Stocker, D., Qin, G.-K., Plattner, M., Tignor, S. K., Allen, J., Boschung, et al. (Eds.), *Climate change 2013: The physical science basis*. Cambridge University Press.

IPCC. (2021). Summary for policymakers. Contribution of working group I to the sixth assessment Report of the intergovernmental panel on climate change. In P., Zhai, A., Pirani, S. L., Connors, C., Péan, S., Berger, N., Caud, et al. (Eds.), *Climate change 2021: The physical science basis*. [Masson-Delmotte, V (pp. 3–32)]. Cambridge University Press.

Jahn, A. (2018). Reduced probability of ice-free summers for 1.5°C compared to 2°C warming. *Nature Climate Change*, *8*(5), 409–413. https://doi.org/10.1038/s41558-018-0127-8

Jahn, A., Kay, J. E., Holland, M. M., & Hall, D. M. (2016). How predictable is the timing of a summer ice-free Arctic? *Geophysical Research Letters*, *43*(17), 9113–9120. https://doi.org/10.1002/2016gl070067

Knutti, R. (2010). The end of model democracy? *Climatic Change*, *102*(3), 395–404. https://doi.org/10.1007/s10584-010-9800-2

Knutti, R., Masson, D., & Gettelman, A. (2013). Climate model genealogy: Generation CMIP5 and how we got there. *Geophysical Research Letters*, *40*(6), 1194–1199. https://doi.org/10.1002/grl.50256

Knutti, R., Sedláček, J., Sanderson, B. M., Lorenz, R., Fischer, E. M., & Eyring, V. (2017). A climate model projection weighting scheme accounting for performance and interdependence. *Geophysical Research Letters*, *44*(4), 1909–1918. https://doi.org/10.1002/2016gl072012

Laliberté, F., Howell, S. E. L., & Kushner, P. J. (2016). Regional variability of a projected sea ice-free Arctic during the summer months. *Geophysical Research Letters*, *43*(1), 256–263. https://doi.org/10.1002/2015gl066855

Lee, W.-L., Wang, Y.-C., Shiu, C.-J., Tsai, I., Tu, C.-Y., Lan, Y.-Y., et al. (2020). Taiwan Earth System Model Version 1: Description and evaluation of mean state. *Geoscientific Model Development*, *13*(9), 3887–3904. https://doi.org/10.5194/gmd-13-3887-2020

Liu, J., Song, M., Horton, R. M., & Hu, Y. (2013). Reducing spread in climate model projections of a September ice-free Arctic. *Proceedings of the National Academy of Sciences*, *110*(31), 12571–12576. https://doi.org/10.1073/pnas.1219716110

Lorenz, R., Herger, N., Sedláček, J., Eyring, V., Fischer, E. M., & Knutti, R. (2018). Prospects and caveats of weighting climate models for summer maximum temperature projections over North America. *Journal of Geophysical Research: Atmospheres*, *123*(9), 4509–4526. https://doi.org/10.1029/2017jd027992

Lukovich, J. V., Stroeve, J. C., Crawford, A., Hamilton, L., Tsamados, M., Heorton, H., & Massonnet, F. (2021). Summer extreme cyclone impacts on Arctic sea ice. *Journal of Climate*, *34*(12), 4817–4834. https://doi.org/10.1175/jcli-d-19-0925.1

Masson, D., & Knutti, R. (2013). Predictor screening, calibration, and observational constraints in climate model ensembles: An illustration using climate sensitivity. *Journal of Climate*, *26*(3), 887–898. https://doi.org/10.1175/jcli-d-11-00540.1

Merrifield, A., Brunner, L., Lorenz, R., & Knutti, R. (2019). A weighting scheme to incorporate large ensembles in multi-model ensemble projections. *Earth System Dynamics Discussion*. https://doi.org/10.5194/esd-2019-69

Notz, D., & Community, S. (2020). Arctic sea ice in CMIP6. *Geophysical Research Letters*, *47*(10), e2019GL086749. https://doi.org/10.1029/2019gl086749

O'Neill, B. C., Tebaldi, C., van Vuuren, D. P., Eyring, V., Friedlingstein, P., Hurtt, G., et al. (2016). The scenario model Intercomparison project (ScenarioMIP) for CMIP6. *Geoscientific Model Development*, *9*(9), 3461–3482. https://doi.org/10.5194/gmd-9-3461-2016

Park, H., Stewart, A. L., & Son, J. (2018). Dynamic and thermodynamic impacts of the winter Arctic oscillation on summer sea ice extent. *Journal of Climate*, *31*(4), 1483–1497. https://doi.org/10.1175/jcli-d-17-0067.1

Rayner, N. A., Parker, D. E., Horton, E. B., Folland, C. K., Alexander, L. V., Rowell, D. P., et al. (2003). Global analyses of sea surface temperature, sea ice, and night marine air temperature since the late nineteenth century. *Journal of Geophysical Research*, *108*(D14), 4407. https://doi.org/10.1029/2002jd002670

Ricker, R., Kauker, F., Schweiger, A., Hendricks, S., Zhang, J., & Paul, S. (2021). Evidence for an increasing role of ocean heat in Arctic winter sea ice growth. *Journal of Climate*, *34*(13), 5215–5227. https://doi.org/10.1175/jcli-d-20-0848.1

Rodgers, K. B., Lee, S.-S., Rosenbloom, N., Timmermann, A., Danabasoglu, G., Deser, C., et al. (2021). Ubiquity of human-induced changes in climate variability. *Earth Syst. Dynam.*, *12*(4), 1393–1411. https://doi.org/10.5194/esd-12-1393-2021

Rosenblum, E., & Eisenman, I. (2017). Sea ice trends in climate models only Accurate in runs with biased global warming. *Journal of Climate*, *30*(16), 6265–6278. https://doi.org/10.1175/jcli-d-16-0455.1

Sanderson, B. M., Knutti, R., & Caldwell, P. (2015a). Addressing interdependency in a multimodel ensemble by interpolation of model properties. *Journal of Climate*, *28*(13), 5150–5170. https://doi.org/10.1175/jcli-d-14-00361.1

Sanderson, B. M., Knutti, R., & Caldwell, P. (2015b). A representative democracy to reduce interdependency in a multimodel ensemble. *Journal of Climate*, *28*(13), 5171–5194. https://doi.org/10.1175/jcli-d-14-00362.1

Sanderson, B. M., Wehner, M., & Knutti, R. (2017). Skill and independence weighting for multi-model assessments. *Geoscientific Model Development*, *10*(6), 2379–2395. https://doi.org/10.5194/gmd-10-2379-2017

Screen, J. A., & Deser, C. (2019). Pacific Ocean variability influences the time of emergence of a seasonally ice-free Arctic ocean. *Geophysical Research Letters*, *46*(4), 2222–2231. https://doi.org/10.1029/2018gl081393

Senftleben, D., Lauer, A., & Karpechko, A. (2020). Constraining uncertainties in CMIP5 projections of september Arctic sea ice extent with observations. *Journal of Climate*, *33*(4), 1487–1503. https://doi.org/10.1175/jcli-d-19-0075.1

Shiru, M. S., & Chung, E.-S. (2021). Performance evaluation of CMIP6 global climate models for selecting models for climate projection over Nigeria. *Theoretical and Applied Climatology*, *146*(1), 599–615. https://doi.org/10.1007/s00704-021-03746-2

Sigmond, M., Fyfe, J. C., & Swart, N. C. (2018). Ice-free Arctic projections under the Paris agreement. *Nature Climate Change*, *8*(5), 404–408. https://doi.org/10.1038/s41558-018-0124-y

Song, M.-R. (2016). Change of Arctic sea-ice volume and its relationship with sea-ice extent in CMIP5 simulations. *Atmospheric and Oceanic Science Letters*, *9*(1), 22–30. https://doi.org/10.1080/16742834.2015.1126153

Thackeray, C. W., & Hall, A. (2019). An emergent constraint on future Arctic sea-ice albedo feedback. *Nature Climate Change*, *9*(12), 972–978. https://doi.org/10.1038/s41558-019-0619-1

Tong, L. I., Zhihong, J., Lilong, Z., & Laurent, L. I. (2020). Multi-model ensemble projection of precipitation changes over China under global warming of 1.5 and 2°C with consideration of model performance and independence. *Journal of Meteorological Research*, *35*(1), 184–197. https://doi.org/10.1007/s13351-021-0067-5

Wang, B., Zhou, X., Ding, Q., & Liu, J. (2021). Increasing confidence in projecting the Arctic ice-free year with emergent constraints. *Environmental Research Letters*, *16*(9), 094016. https://doi.org/10.1088/1748-9326/ac0b17

23284277, 2022, 10, Downloaded from https://agupubs.onlinelibrary.wiley.com/doi/10.1029/2022EF002708 by Universitetsbiblioteket I, Wiley Online Library on [29/12/2022]. See the Terms and Conditions (https://onlinelibrary.wiley.com/terms-and-conditions) on Wiley Online Library for rules of use; OA articles are governed by the applicable Creative Commons License

Wang, M., & Overland, J. E. (2009). A sea ice free summer Arctic within 30 years? *Geophysical Research Letters*, *36*(7). https://doi.org/10.1029/2009gl037820

Wang, M., & Overland, J. E. (2012). A sea ice free summer Arctic within 30 years: An update from CMIP5 models. *Geophysical Research Letters*, *39*(18). https://doi.org/10.1029/2012gl052868

Weigel, A. P., Knutti, R., Liniger, M. A., & Appenzeller, C. (2010). Risks of model weighting in multimodel climate projections. *Journal of Climate*, *23*(15), 4175–4191. https://doi.org/10.1175/2010jcli3594.1

Yang, X., Zhou, B., Xu, Y., & Han, Z. (2021). CMIP6 evaluation and projection of temperature and precipitation over China. *Advances in Atmospheric Sciences*, *38*(5), 817–830. https://doi.org/10.1007/s00376-021-0351-4

Zhao, J., He, S., & Wang, H. (2022). Historical and future runoff changes in the Yangtze River Basin from CMIP6 models constrained by a weighting strategy. *Environmental Research Letters*, *17*(2), 024015. https://doi.org/10.1088/1748-9326/ac3f61

Erratum

The following errors were discovered in the author affiliations in the supporting information after publication of this paper: Affiliation 4 was incorrectly listed as "Southern Marine Science and Engineering Guangdong Laboratory (Zhuhai), Zhuhai, People's Republic of China", and affiliation 5 was incorrectly listed as "Nansen Environmental and Remote Sensing Center and Bjerknes Centre for Climate Research, Bergen, Norway". The author affiliations have been corrected, and this may be considered the authoritative version of record.

23284277, 2022, 10, Downloaded from https://agupubs.onlinelibrary.wiley.com/doi/10.1029/2022EF002708 by Universitetsbiblioteket I, Wiley Online Library on [29/12/2022]. See the Terms and Conditions (https://onlinelibrary.wiley.com/terms-and-conditions) on Wiley Online Library for rules of use; OA articles are governed by the applicable Creative Commons License